

PAPER

In vitro model to study confined osteocyte networks exposed to flow-induced mechanical stimuli

To cite this article: Kairui Zhang *et al* 2022 *Biomed. Mater.* **17** 065027

View the [article online](#) for updates and enhancements.

You may also like

- [Biofabrication of vasculature in microphysiological models of bone](#)
Ian T Whelan, E Moeendarbary, David A Hoey *et al.*
- [Effect of external mechanical stimuli on human bone: a narrative review](#)
Megan E Mancuso, Andrew R Wilzman, Kyle E Murdock *et al.*
- [Advantages of microfluidic systems for studying cell-biomaterial interactions—focus on bone regeneration applications](#)
Gemma Mestres, Roman A Perez, Noelia Laura D'Elia *et al.*



Breath Biopsy[®] OMNI

The most advanced, complete solution for global breath biomarker analysis

SEE WHAT OMNI
CAN DO FOR YOU



Expert Study Design
& Management



Robust Breath
Collection



Reliable Sample
Processing & Analysis



In-depth Data
Analysis



Specialist Data
Interpretation

Biomedical Materials



PAPER

In vitro model to study confined osteocyte networks exposed to flow-induced mechanical stimuli

Kairui Zhang^{1,2}, Courtney Ogando^{1,2}, Alex Filip^{1,2}, Teng Zhang^{2,4}, Jason A Horton^{2,3}  and Pranav Soman^{1,2,*} 

¹ Department of Biomedical and Chemical Engineering, Syracuse University, Syracuse, NY 13244, United States of America

² Syracuse Biomaterials Institute, Syracuse, NY 13244, United States of America

³ Department of Orthopedic Surgery, SUNY Upstate Medical University, Syracuse, NY 13210, United States of America

⁴ Department of Mechanical and Aerospace Engineering, Syracuse University, Syracuse, NY 13244, United States of America

* Author to whom any correspondence should be addressed.

E-mail: psoman@syr.edu

Keywords: *in vitro* model, osteocyte, calcium signaling, heterogeneity, flow stimuli, confinement, gap-junction

Supplementary material for this article is available [online](#)

RECEIVED
17 August 2022

REVISED
11 November 2022

ACCEPTED FOR PUBLICATION
16 November 2022

PUBLISHED
25 November 2022

Abstract

Osteocytes are considered the primary mechanical sensor in bone tissue and orchestrate the coupled bone remodeling activity of adjacent osteoblast and osteoclast cells. *In vivo* investigation of mechanically induced signal propagation through networks of interconnected osteocytes is confounded by their confinement within the mineralized bone matrix, which cannot be modeled in conventional culture systems. In this study, we developed a new model that mimics this *in vivo* confinement using gelatin methacrylate (GelMA) hydrogel or GelMA mineralized using osteoblast-like model cells. This model also enables real-time optical examination of osteocyte calcium (Ca^{2+}) signaling dynamics in response to fluid shear stimuli cultured under confined conditions. Using this system, we discovered several distinct and previously undescribed patterns of Ca^{2+} responses that vary across networks of interconnected osteocytes as a function of space, time and connectivity. Heterogeneity in Ca^{2+} signaling may provide new insights into bone remodeling in response to mechanical loading. Overall, such a model can be extended to study signaling dynamics within cell networks exposed to flow-induced mechanical stimuli under confined conditions.

1. Introduction

It is widely accepted that osteocytes comprising more than 90% of all bone cells are responsible for sensing and transducing mechanical stimuli and integrating hormonal signals to coordinate bone remodeling and homeostasis [1–3]. Mechanical loading of bone induces interstitial fluid flow at the cellular level. The resulting fluid shear force is sensed by osteocytes and propagated across the lacunar-canalicular network (LCN) along dendritic processes that connect cells via gap junctions and/or soluble biochemical signals [4–9] (figure 1(A)). Since disrupted osteocyte signaling has been implicated in variety of physiological skeletal disorders, an in-depth understanding of osteocyte signaling is necessary [10–21]. However,

real-time observation of signaling across the osteocyte network has been challenging due to their location within opaque calcified bone matrix [8, 22–24].

Direct visualization of osteocyte signaling has historically involved observation of live bone explants or living animals. However, these procedures typically require extensive manipulation to enable perfusion of fluorescent tracers, and complex apparatus allowing loading and imaging for immediate analysis by time-lapse microscopy [25–27]. Such approaches enforce tight experimental timelines and have limited capacity to examine multiple samples in parallel (e.g. drug response). Furthermore, these systems can be confounded by anatomic variability of specimens, inconsistent tracer perfusion, cardiac/respiratory motion artifacts, as well as limited depth of field for optical

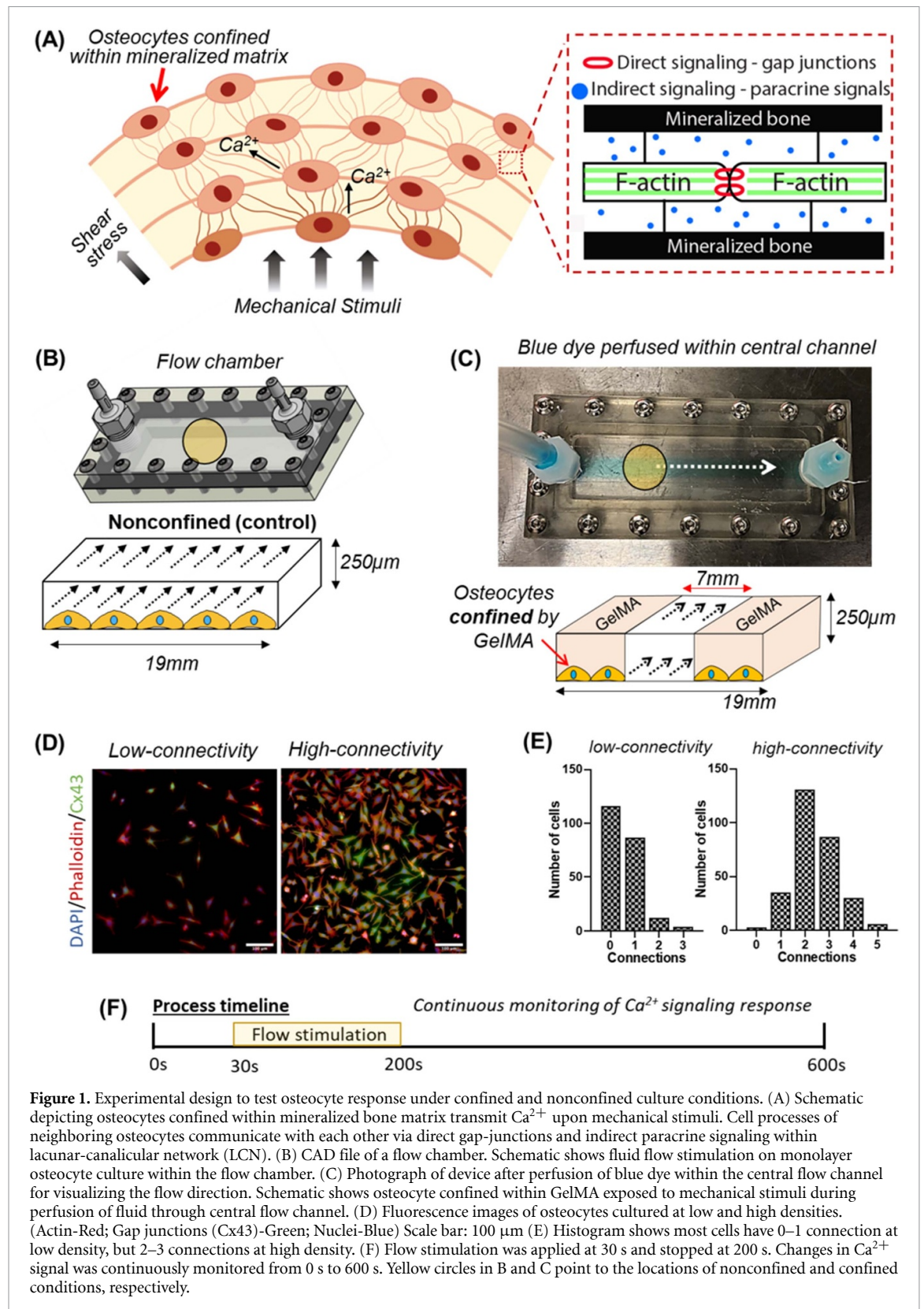


Figure 1. Experimental design to test osteocyte response under confined and nonconfined culture conditions. (A) Schematic depicting osteocytes confined within mineralized bone matrix transmit Ca^{2+} upon mechanical stimuli. Cell processes of neighboring osteocytes communicate with each other via direct gap-junctions and indirect paracrine signaling within lacunar-canalicular network (LCN). (B) CAD file of a flow chamber. Schematic shows fluid flow stimulation on monolayer osteocyte culture within the flow chamber. (C) Photograph of device after perfusion of blue dye within the central flow channel for visualizing the flow direction. Schematic shows osteocyte confined within GelMA exposed to mechanical stimuli during perfusion of fluid through central flow channel. (D) Fluorescence images of osteocytes cultured at low and high densities. (Actin-Red; Gap junctions (Cx43)-Green; Nuclei-Blue) Scale bar: 100 μ m (E) Histogram shows most cells have 0–1 connection at low density, but 2–3 connections at high density. (F) Flow stimulation was applied at 30 s and stopped at 200 s. Changes in Ca^{2+} signal was continuously monitored from 0 s to 600 s. Yellow circles in B and C point to the locations of nonconfined and confined conditions, respectively.

imaging. As a result, several *in vitro* models varying in the degree of complexity have been developed. Easy to use, two-dimensional platforms such as well plates, laminar flow chambers, or micropatterning methods [28], and microfluidic devices [29–31], have been used to apply shear forces to osteocyte monolayers [32–34]. In a typical setup, osteocytes are cultured

on a glass slide, and rockers, shakers or external pumps are used to generate defined flow profiles. To recapitulate *in vivo* like 3D confinement of osteocytes within bone tissue, osteocytes have been encapsulated within a hydrogel matrix (e.g. collagen, fibrin, basement membrane extracts) [35–42], or have been cultured on the surfaces of 3D microbead assemblies

[41]. However, quantitative real-time live cell imaging of osteocyte networks within these 3D constructs has been difficult due to the cells being in different planes and similar attenuation of excitation/emission photons with increasing penetration depth into the gel [43].

To balance the needs of mimicking physiological complexity and real-time observation of signaling dynamics across networks of interconnected osteocytes, we developed a flow-chamber-based model that enables both time-lapse fluorescence imaging and the application of fluid shear stimuli under matrix-confined or non-confined conditions. For these experiments, we evaluated the dynamics Ca^{2+} signal generation and propagation in the model osteocyte-like cell line Murine osteocyte-like cell line MLO-Y4 (MLO-Y4) [44]. Confined conditions were generated by overlaying monolayers of MLO-Y4 osteocytes with photo-crosslinkable gelatin methacrylate (GelMA) or GelMA mineralized *in situ* by encapsulated osteoblast like cells (Saos-2). Using this system, we identified distinct spatio-temporal patterns of fluid shear-evoked Ca^{2+} responses across the network of osteocytes, which varied as a function of their location and confinement conditions. To our knowledge, this is first report to identify and characterize heterogeneity in Ca^{2+} response and signal propagation across a network of matrix-confined osteocytes. Considering the significance of intracellular Ca^{2+} signaling in many biological processes [45, 46], we expect this work will lead to yet undiscovered insights into how osteocytes transduce mechanical stimuli to orchestrate bone remodeling and homeostasis.

2. Results

2.1. Experimental design

To generate *in vivo* like conditions, we developed an *in vitro* model using a custom-built flow chamber to study osteocyte networks under ‘confined’ and ‘non-confined’ conditions. (SI-figure 1) In the ‘non-confined’ condition (figure 1(B)), osteocytes are directly stimulated by fluid flow passing directly over the cell monolayer, in the manner of a traditional laminar flow chamber. In contrast, under the confined condition, the fluid flow stimulus is restricted to be experienced only by cells at the fluid-matrix interface as media passes through the flow chamber (figure 1(C)). We hypothesized that, under confined conditions, osteocytes at the interface of the channel directly receive fluid shear stimulation and relay this stimulus along dendritic processes via gap junctions and/or paracrine signals to cells further removed from the channel wall. Perfusion of 0.1 mg ml^{-1} Fluorescein isothiocyanate (FITC)-dextran 20 kDa into the chip showed only slight diffusion in the gel for time-points relevant for this study (300 s, SI-figure 2). For these experiments, we set the shear stress in the

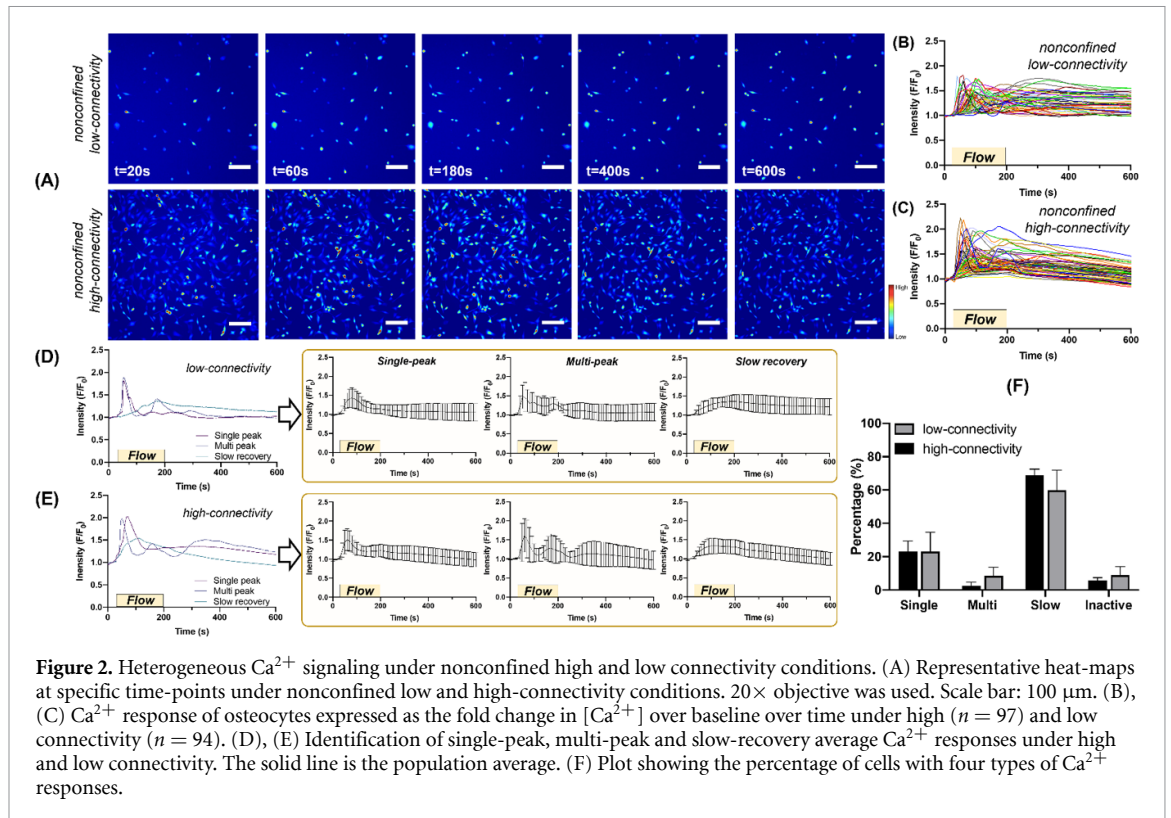
channel to be $\sim 0.85 \text{ Pa}$. Numerical simulation results carried out with ABAQUS/Implicit shows that shear stress experienced by monolayer of osteocytes confined under GelMA hydrogel is between a narrow range of 0.85–0.81 Pa; these values are at the lower side of the 0.8–3 Pa range reported in the literature [47] (SI-figure 3). To study the role of cellular connectivity in Ca^{2+} signaling, osteocytes were seeded at both high and low density (figure 1(D)), and the number of direct cell–cell connections were counted for individual cells. In low density condition, most osteocytes directly contact one or fewer cells, while in high density most osteocytes directly contact two or more cells (figure 1(E)). This suggests that only few cells in low density can transmit Ca^{2+} signals via gap junction. The fluid flow stimulation was performed according to a designed timeline (figure 1(F)). Ca^{2+} signals were recorded during the entire duration of the experiment.

2.2. Heterogeneous Ca^{2+} signaling under non-confined conditions

Timelapse fluorescence imaging showed an increase in Ca^{2+} levels over time upon flow stimulation under both non-confined high and low connectivity conditions (figure 2(A)). After normalizing the fluorescence intensity to baseline data collected for 30 s before flow stimulation was applied, three types of Ca^{2+} signals were identified: single peak, multi-peak and slow recovery (figures 2(D) and (E)). ‘Single peak’ cells exhibit a rapid Ca^{2+} signal peak upon flow stimulation. ‘Multi-peak’ cells have more than one peak with decreasing peak height in second or third spike. ‘Slow recovery’ cells show delayed peak and slower recovery with full width at half maximum (FWHM) greater than 120 s. ‘Inactive’ cells which showed no increase in Ca^{2+} intensity upon stimulation were also characterized. Under high connectivity condition, ‘single peak’ (23%) and ‘slow recovery’ (69%) were found to be dominant cellular responses as compared to ‘multi-peak’ (2%) and ‘inactive’ (6%). Under low connectivity condition, ‘single peak’ and ‘slow recovery’ cells account for 23% and 60% respectively, while ‘multi-peak’ and ‘inactive’ only account for 8% and 9% (figure 2(F)). We further quantified maximum peak intensity, time to peak, FWHM, peak interval and final intensity of all the active cells (SI, figure 4). Although most of the parameters were at similar levels in both conditions, it took longer time for ‘single peak’ cells (30 s vs 46 s, $p = 0.008$) and ‘slow recovery’ cells (109 s vs 160 s, $p = 0.0004$) to reach signal peak under low connectivity.

2.3. Heterogeneous Ca^{2+} signaling under confined conditions

To mimic *in vivo* physiology of bone, where osteocytes embedded within bone matrix indirectly sense and respond to flow-induced mechanical stimuli, Ca^{2+}



signaling response of osteocyte monolayers confined under crosslinked GelMA was investigated. An increase in Ca^{2+} fluorescence intensity was detected for most cells at high connectivity (figures 3(A) and (C)), while few cells (figure 3(D)) are active under low connectivity conditions. Under confinement and low connectivity conditions, active cells were primarily found directly adjacent to the fluid interface, while those located away from the channel were largely inactive. At cell high density, however, Ca^{2+} release was observed throughout the construct. This indicates that cells at the fluid interface can initiate the mechanotransductive signal, but further propagation requires downstream cells to be in direct contact or in proximity. Therefore, we focused on cells at high connectivity condition for remainder of the study.

Among actively signaling cells, we observed three distinct patterns Ca^{2+} response: ‘single peak’, ‘slow recovery’ and ‘plateau’ (figure 3(E)). As ‘single peak’ and ‘slow recovery’ responses appear in both confined and non-confined conditions, we analyzed the Ca^{2+} signal wave form for each cell in terms of its maximum intensity, time to peak and FWHM. Osteocytes under confined conditions exhibit similar amplitude of Ca^{2+} peak but a delayed response as compared to non-confined conditions (figures 3(F) and (G)). This can be attributed to indirect stimulation of osteocytes under confined conditions. In the confined condition, a new osteocyte response coined as ‘plateau’ was identified. The plateau response was

defined as no Ca^{2+} intensity decay (less than 0.05) after reaching maximum intensity (figure 3(H)). Under the confined condition, ‘plateau’ cells make up the majority (41%) followed by ‘slow recovery’ (24%) and ‘single peak’ (9%) (figure 3(I)). This response does not appear under non-confined conditions.

2.4. Zone-dependent cellular response

To further investigate how transmission distance affects cellular response, we divided the confined area into two zones: proximal Zone 1 (0–200 μm from channel interface) and distal Zone 2 (200–400 μm away from the interface). We observed that signal propagation occurred as a wave initiating at the channel interface, gradually moving away, first through the Zone 1 and then Zone 2 (figure 4(A)). Comparing the Ca^{2+} signal form between zones revealed a significantly higher percentage of ‘Plateau’ cells in Zone 2 (63% vs 19%, $p = 0.0007$), and fewer ‘single peak’ (2% vs 16%, $p = 0.0003$) and ‘slow recovery’ (9% vs 38%, $p = 0.0024$) than in Zone 1 (figure 4(B)). These results indicate that the proximal single peak and slow recovery responses may result from direct stimulation by fluid flow, and subsequently propagate distally to the plateau cells that predominate in Zone 2. We further compared maximum intensity and time to peak of all three types in both zones. Although no significant differences were found in ‘single peak’ cell between the zones

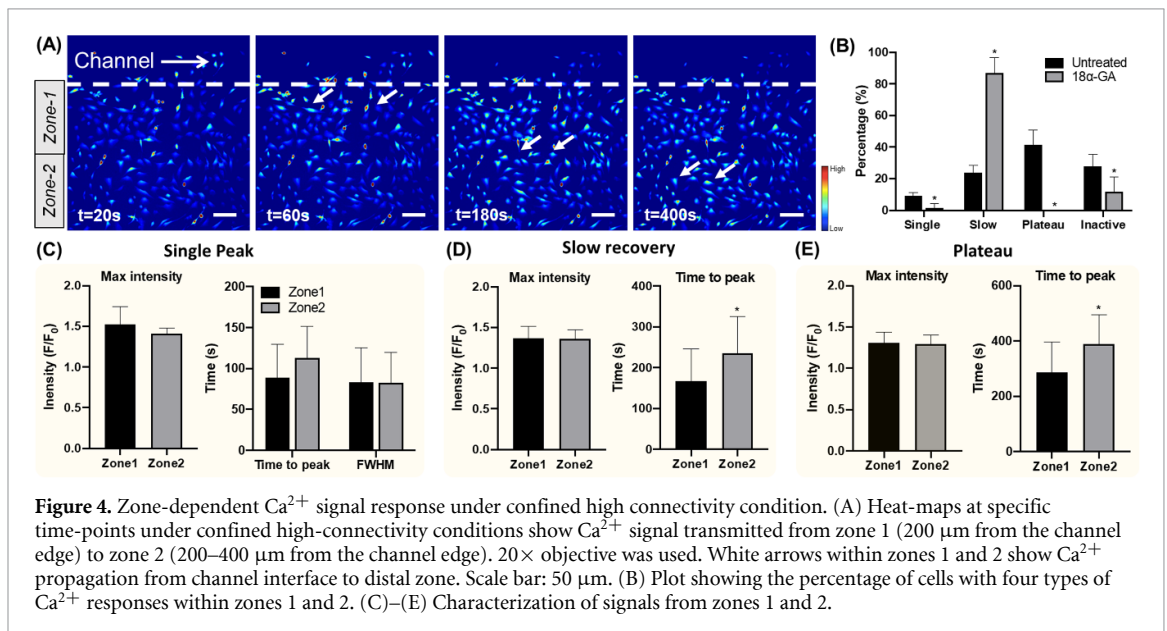
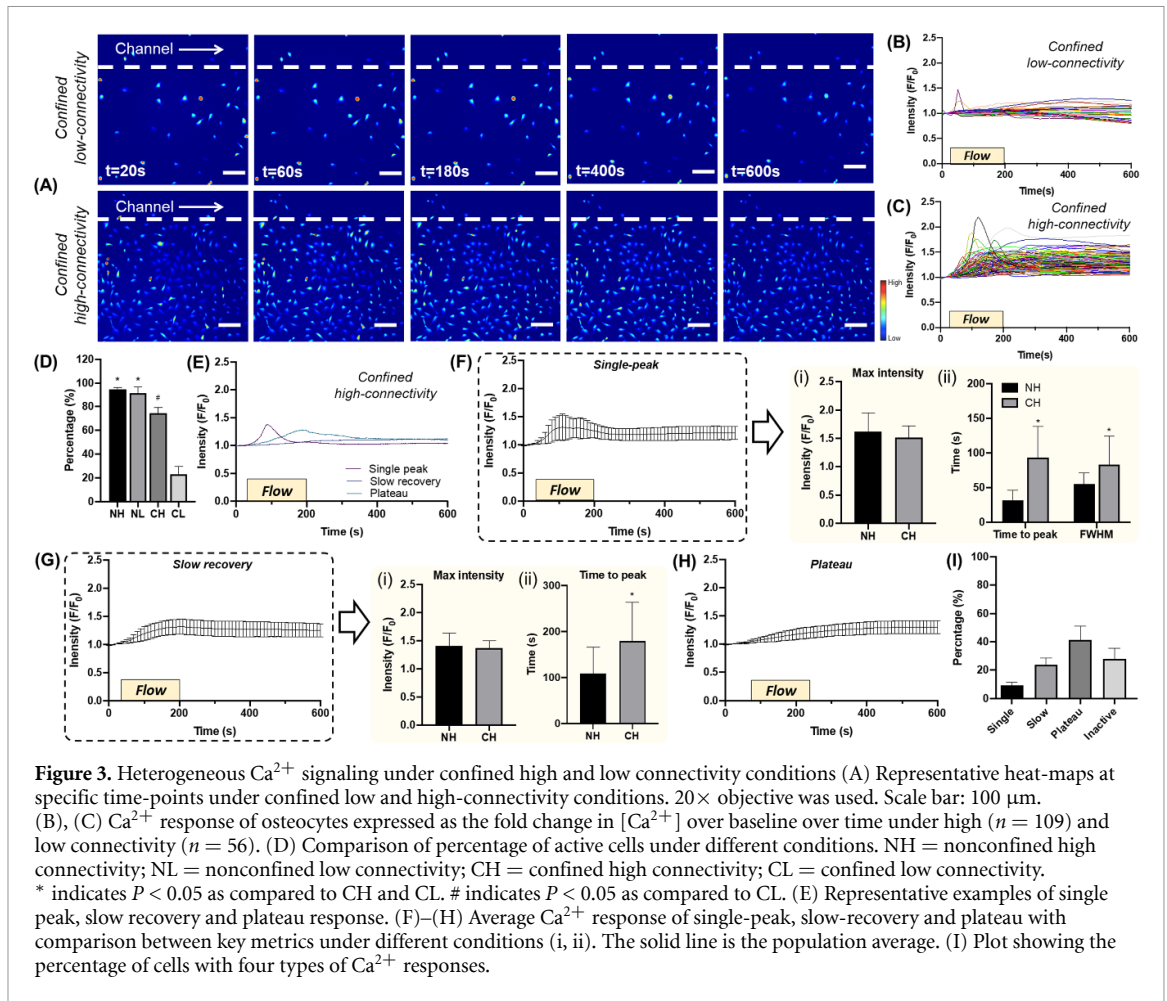
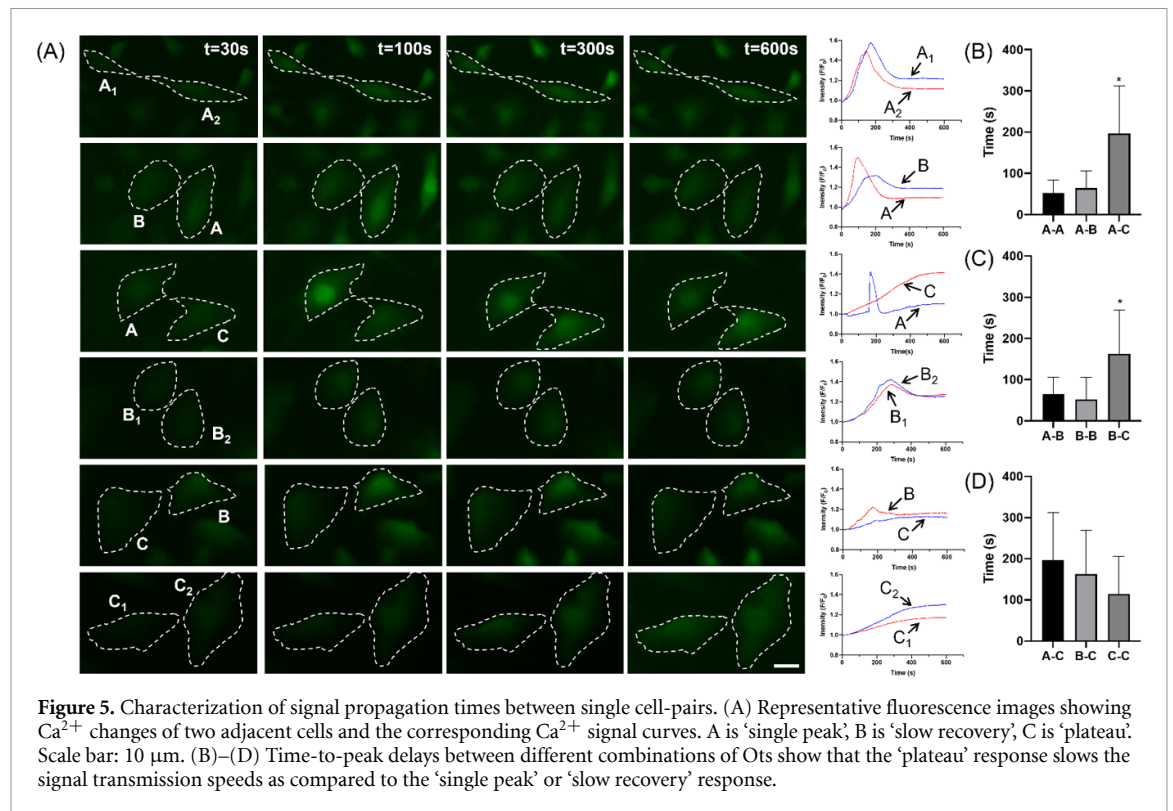


(figure 4(C)), both ‘slow recovery’ and ‘Plateau’ show a delayed time to peak response in the distal zone, ultimately achieving similar maximum intensity in both zones (figures 4(D) and (E)). Next, signal propagation times between single cell-pairs that exhibit same or different types of Ca^{2+} responses were investigated

(figure 5(A)). In this case, only cells with physical contact to another cell were evaluated. Results show high propagation speeds for cell pairs that exhibit single peak or slow-recovery responses while slow speeds when one of the cells in the pair exhibits a plateau response (figures 5(B)–(D)). In parallel,



a computational model was developed to represent cell–cell signal propagation under confined conditions (SI, figure 5). In our computational model, the first osteocyte in a chain of cells is identified as 'mechanically stimulated cell'; this represents osteocytes at the channel edge that will be subjected to direct flow stimuli. Osteocytes downstream of the mechanically stimulated cells are identified as 'chain stimulation cells'; this represents osteocytes deeper inside GelMA layer. By varying specific kinetic parameters, we were able to match computational modeling results to experimentally observed 'single peak' and 'slow recovery' Ca^{2+} responses between osteocyte cell pairs (SI, figures 5(C) and (D)). The details of the model are provided in SI information.

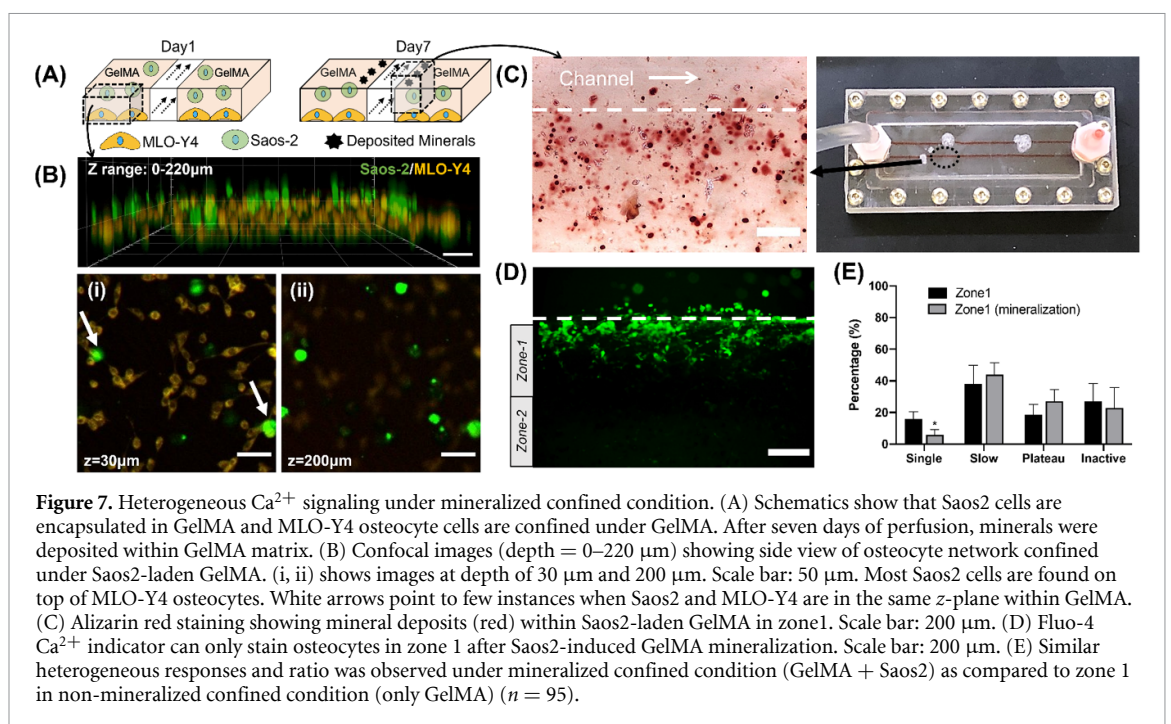
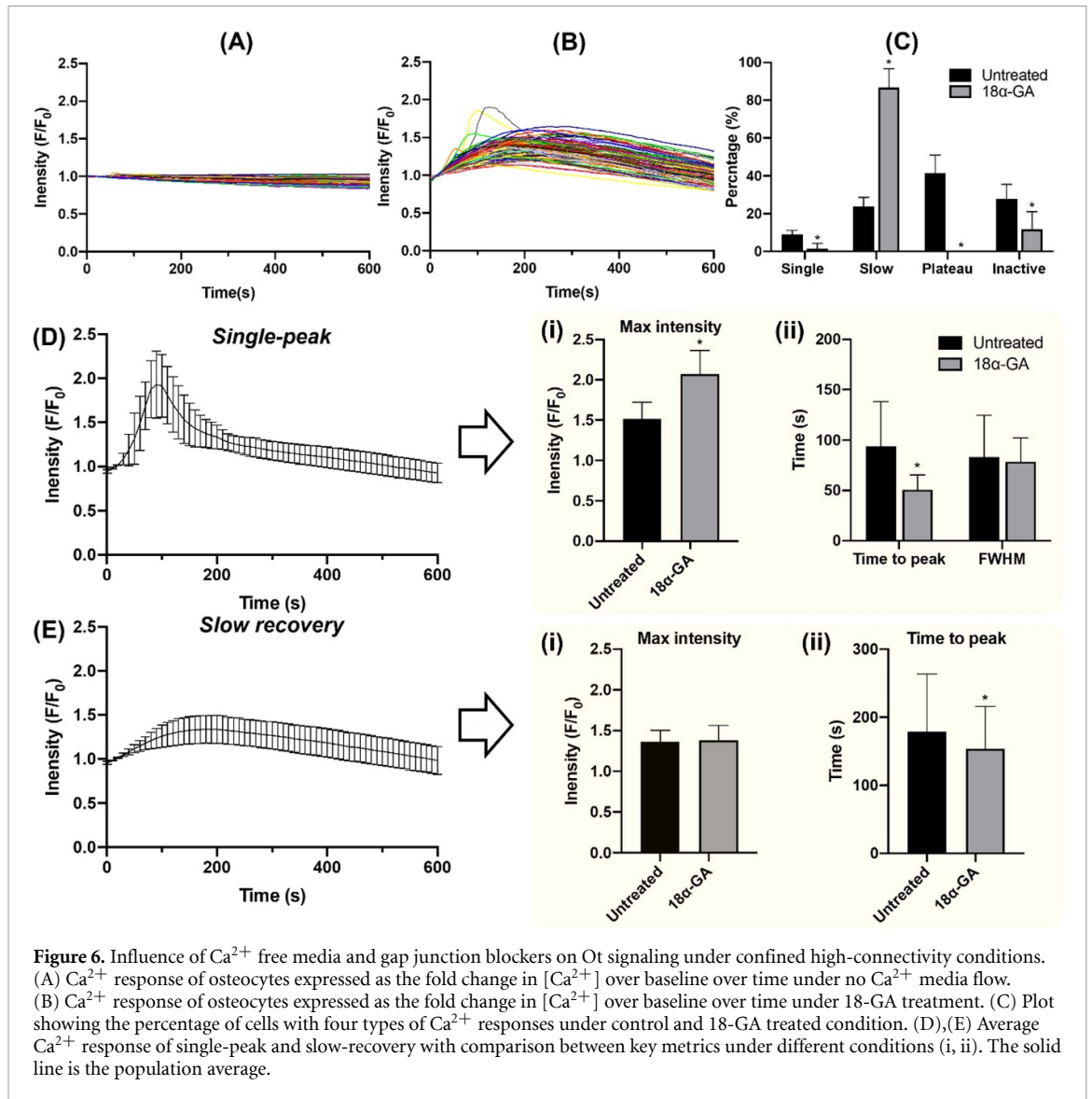
2.5. Influence of extracellular Ca^{2+} depletion and gap junction blockers on osteocyte signaling under confined, high-connectivity conditions

Given that high-cell density was required for signal propagation away from the fluid interface, we examined whether the signal propagation mechanisms may contribute to heterogeneity of Ca^{2+} responses. It is well understood that spikes in cytoplasmic Ca^{2+} can result from either extracellular Ca^{2+} influx or release from the endoplasmic reticulum (ER). To determine whether extracellular influx contributed to the Ca^{2+} response to flow stimuli, we repeated our experiments using Ca^{2+} free media. Under these conditions, the Ca^{2+} response to flow stimulation (figure 6(A)) was abolished, indicating that extracellular influx Ca^{2+} is necessary for signal initiation and propagation. This insight is valuable in

diseases where the numeric density of viable osteocytes, and therefore their connectivity, is reduced (e.g. osteoporosis, osteonecrosis), such that the efficiency and dynamics of signal propagation in response to loading could be altered, adversely affecting the remodeling response of osteoblasts and osteoclasts. To test how gap junctional communication contributes to cell signal heterogeneity, we treated osteocytes with 18-Glycyrrhetic acid (18-GA), a gap junction inhibitor before starting flow stimulation. Interestingly, when gap junctions were blocked, the number of active cells did not change, but their Ca^{2+} response changed from 'plateau' to a 'slow recovery' wave form (figures 6(B) and (C)). We further compared the maximum intensity and time to peak between control and treated group. The results show an increase in 'single' peak intensity and time delay in both 'single' and 'slow recovery' (figures 6(D) and (E)). This indicates that, following the initial rise, cells that exhibit 'plateau' response require supply of Ca^{2+} from neighboring cells through gap junctions to maintain a stable Ca^{2+} signal and when gap junctions are blocked these cells may default to the 'slow recovery' wave form.

2.6. Cellular response under mineralized confined condition

Although GelMA provides a barrier for the cells to be directly exposed to flow stimulation, a mineralized matrix may better mimic the osteocyte network *in vivo*. Thus, we encapsulated Saos-2, an osteoblast-like cell line, within GelMA matrix and induced them to mineralize the confining matrix above the osteocyte monolayer (figure 7(A)). The confocal



images show Saos2 distributed within GelMA on top of osteocyte monolayer (figure 7(B)). After seven days of osteogenic perfusion, the Alizarin red staining result shows mineralization within zone 1 (0–200 μm) (figure 7(C)). Ca^{2+} signal responses of osteocytes under mineralized GelMA are like those under (unmineralized) GelMA, although osteocytes demonstrate significantly fewer ‘single peak’ cells (16% vs 6%, $p = 0.016$) (figures 7(D) and (E)).

3. Discussion

Fluid flow is sensed as shear stress by the primary cilia and/or through deformation of the osteocyte cytoskeleton, eliciting a rapid rise in intracellular calcium (Ca^{2+}) [48, 49]. Ca^{2+} signaling, a ubiquitous second messenger mechanism, regulates many downstream cellular activities in response to physical stimuli, and can be transmitted as a signal between cells via gap junction channels [50, 51]. While many *in vitro* models allow real-time observation of Ca^{2+} signaling upon stimulation, none of the existing models focus on how Ca^{2+} signaling is propagated between cells in an confined environment. For instance, parallel-plate flow chambers have been widely used to investigate real-time signaling responses to fluid shear stimuli [52–56]. Although conventional oscillatory or pulsatile flow approaches have been developed to mimic fluid flow patterns experienced *in vivo*, these systems directly stimulate all cells in the flow chamber. As a result, the ability to capture signal propagation from individual, directly stimulated cells across networks connected but indirectly stimulated downstream cells is confounded. In this work, we developed an *in vitro* model that: (a) recapitulates the confinement of osteocytes with defined connectivity in a gelatin-based extracellular matrix with or without osteoblast-mediated mineralization, (b) restricts mechanical stimuli to the osteocytes at the fluid-matrix interface and (c) allows real-time imaging of dynamic cellular signaling events. Confinement was achieved by overlaying the osteocyte monolayer with a photopolymerizable GelMA matrix. The GelMA matrix was selected because it chemically resembles the native collagenous bone matrix, contains integrin attachment sites that facilitate interaction of the cytoskeleton and matrix through focal adhesions, and is conducive to mineralization by embedded osteoblastic cells as we have shown previously [57–59]. Connectivity of the osteocytes can be manipulated by varying the seeding density of the osteocytes. The central flow chamber restricts direct exposure to the fluid shear stimulus to those cells at the channel interface, allowing their mechanotransduced signal to propagate to other cells located deeper within the construct. Finally, this new model system uses a monolayer of osteocytes within a uniform optical plane that allows precise spatial and

temporal resolution of Ca^{2+} signaling dynamics for several hundred cells in a single imaging session. In initial experimental design, the real-time imaging was stopped by the end of flow stimulation (200 s). However, our results showed that few Ca^{2+} signals kept increasing till the end of experiments under confined high connectivity condition (SI, figure 6). Hence, we extended the observation time to 600 s.

Intracellular Ca^{2+} signaling resulting from mechanical stimulation has been widely studied in osteocytes *in vitro* or by using live bone explants. Most existing studies typically report single peak or spike response that is characterized by rapid rise in fluorescence intensity of Ca^{2+} markers when subjected to mechanical stimuli [60], and cells are classified as ‘active’ or ‘inactive’. For instance, Adachi *et al* found that osteocytes in calvaria deformed by using a needle showed a rapid and prolonged increase of Ca^{2+} concentration [61]. Jing *et al* found that osteocytes in explanted mouse tibiae displayed repetitive Ca^{2+} spikes in response to cyclic loading [60]. However, none have reported heterogeneity of fluid shear evoked Ca^{2+} waveforms for single cells, nor the impact of this heterogeneity signal propagation between adjacent cells, that we have shown here. Similar variations in frequencies, amplitudes and waveforms including ‘single-’ and ‘multi-peak’, ‘plateau’ and ‘slow recovery’ in Ca^{2+} signaling have been reported in other cell types, such as neurons, endothelial cells, epithelial cell sheets or osteoblastic primary cells [62–65].

Once induced by fluid flow, several factors are reported to be involved in Ca^{2+} release and signal propagation. Primary cilia and focal adhesions can act as mechanosensors [49, 66, 67]; extracellular Ca^{2+} influx through mechanical-sensitive ion channels [68, 69]; Ca^{2+} transmission through gap junction [70, 71]; and paracrine signaling induced Inositol 1,4,5-triphosphate (IP3) binding and Ca^{2+} release from ER [55, 72] (SI, figure 7) may contribute. In our study, similar results were shown in non-confined cells at low and high connectivity, indicating Ca^{2+} exchange between adjacent cells plays an insignificant role in Ca^{2+} spike as compared to the initial Ca^{2+} influx. Our results of 18-GA treatment show that the ‘plateau’ is a gap junctional communication based cellular response. Combining the trend of ‘slow recovery’ and ‘plateau’, we propose that gap junctional Ca^{2+} exchange acts after extracellular influx and IP3 induced Ca^{2+} release to maintain intracellular Ca^{2+} levels in ‘plateau’ cells once peak is achieved. The results that Ca^{2+} peak exhibits a zone-dependent time delay also suggests paracrine signaling induced intracellular Ca^{2+} release predominates, as the speed of paracrine signaling is proportional to distance. Another question is whether ‘single peak’ and ‘slow recovery’ cells behave differently as both types appear at all conditions. One possibility is that primary cilia

or focal adhesion mediated sensing in nonconfined conditions or at the fluid-matrix interface initiates the extracellular Ca^{2+} influx detected as a 'single peak' or slow-recovering signals but cells further with the confining matrix assume the plateau phenotype due to a combination of paracrine and gap junction propagation mechanisms.

In our model, three-dimensional confinement is achieved by overlaying a biomimetic GelMA matrix so that only cells at the channel wall interface are exposed to fluid shear stimulus, allowing observation of Ca^{2+} propagation across a network of monotypic osteocytes naïve to the mechanical stimulus. In contrast, Yvanoff and Willaert use a micropatterning approach to create spatial confinement between adjacent spots of MC3T3-E1 osteoblasts and MLO-Y4 osteocytes, allowing measurement of intracellular Ca^{2+} levels either under fluid shear or nanoindentation stimuli [30]. Importantly, while both nanoindentation and fluid shear stimuli evoke Ca^{2+} release, they do so by activating different response mechanisms (focal-adhesion and primary cilia, respectively) that utilize different repertoire of Ca^{2+} channels that mediate extracellular calcium influx through voltage gated channels or from intracellular stores released from the ER via IP3R or RyR channels. Their nanoindentation experiments showed Cx43 gap junctions mediate Ca^{2+} signal propagation stimulated in osteocytes and non-stimulated osteoblasts, similar to others in the field [73]. In their fluid shear stimulation experiment, spatially confined cell spots were both exposed to the fluid shear, in a manner that was essentially equivalent to our non-confined condition lacking the GelMA overlay. Both their 'spatially confined' and our non-confined experiments showed synchronous Ca^{2+} responses occurred across the field of directly stimulated cells. However, yet there appeared to be no difference in the Ca^{2+} dynamics, for either cell type at heterotypic junctions, when compared to their respective monotypic response to fluid shear. We suspect that this is because all cells observed were exposed to the fluid shear stimulus, thus preventing observation of signal propagation between stimulated and non-stimulated cells, as our systems allows. Furthermore, Yvanoff and Willaert did not report on waveform heterogeneity in their experiments, reinforcing the novelty of this finding in the current study.

The presence of cells with a plateau response and their resistance to signal propagation as compared to the other types is not clear. Our data indicate that the slow recovery phenotype predominates in both unconfined cells (figure 2) and confined cells close to the channel wall (figure 4, Zone 1), though there is a large difference in the kinetics(time-to-peak) between them (figure 3(G-ii), exact values given below) In contrast the 'plateau' phenotype predominates at greater

distances from the channel wall (Zone 2), and display an even longer time-to-peak (~ 400 s, figure 4(E)). Furthermore, that the plateau phenotype disappears upon 18-GA treatment (figure 6(C)), suggests that the sustained Ca^{2+} signal in 'plateau' cells is sustained by continuous signaling transduced via Cx43 gap junctions. That there is no difference in peak signal intensity between slow recovery and plateau in either condition cells suggest no intrinsic difference of intracellular calcium stores as a function of confinement. It is also possible that confinement may provoke differences in the ability of the cells to normalize cytosolic Ca^{2+} either by outward flow or recovery by the ER. However, we have not tested this possibility, nor can we infer from the literature that these mechanisms would be altered by matrix confinement. Divergent Ca^{2+} waveforms between confined and unconfined conditions may also be due to differences in cytoskeletal signaling originating from activation of focal-adhesion/integrin complexes, or reduced cellular deformation that activates Ca^{2+} release via Piezo1 or Trpv4 channels [74, 75].

While we did not examine other potentially relevant signaling mechanisms in the current paper, this simple model can also be extended to other virtually any other mechano-responsive cell types, signals (voltage, adenosine, glutamate, ROS), other relevant physiometric mechanical stimuli (range of shear stresses, oscillatory or pulsatile flow modulation of matrix stiffness), and inclusion of key biomolecules (growth factors) or drugs. Our platform provides a unique means to study spatial and temporal release of transient molecules, and propagation of their respective signals across a network of connected osteocytes. In this study we have used the MLO-Y4 cell line as a model of osteocyte mechanotransduction and have applied consistent stimulation. It has been shown that differentiative heterogeneity is minimal with MLO-Y4 cell line, as compared to cells primary cells or those induced to differentiate from a more primitive state [44, 76]. Since MLO-Y4 are at approximately uniform in their stage of osteocytic differentiation, neither reverting to an immature stage, nor appear to proceed beyond this terminally differentiated state, we reason that the observed Ca^{2+} waveform heterogeneity heterogeneous response is independent of the differentiation stage of osteocytes. The fact that response heterogeneity in the threshold to activate Ca^{2+} response appears in both confined and non-confined conditions may indicate that this is an intrinsic feature of this cell line, and will require further validation, for example with primary human osteocytes, to better understand the relevance of this finding to the maintenance of bone homeostasis *in vivo*. Also, the effect of different amplitude/frequency of stimulation, variations in culture condition or differentiation stage (in case of primary osteocytes) or defined spatial

organization of osteocytes, on the observed heterogeneous responses are needed. Our results show that the cell-induced mineralized matrix has no significant influence on the heterogeneous response. However, more detailed work, such as computational modeling, are required to elucidate how a flow that is applied through a mineralized gel in touch with osteocyte layers compares to a fluid flow within LCN where there is only very narrow space between the cytoskeleton and lacunar wall. While our results reveal that the heterogeneous response of osteocytes are related to various Ca^{2+} release/influx pathways, how cells would integrate these different mechanisms in response to mechanical cues remains an open question. More experiments including blockage of specific ion channels, depletion of stored intracellular Ca^{2+} need to be done for better elucidate the heterogeneous Ca^{2+} signaling mechanism. From a computational perspective, the model remains under development, and we are accumulating additional experimental data to validate the model of mechanically-induced signal propagation across osteocyte networks. We envision that, once developed, such models will be valuable to study signaling dynamics via an organized osteocyte network subjected to spatiotemporally varying stimuli, or genetic models of bone pathology.

To better mimic the *in vivo* like mineralized microenvironment, we co-cultured Saos-2, an osteoblast-like cell line, within GelMA matrix and induced them to mineralize the confining matrix above the osteocyte monolayer (figure 7). Brightfield image (SI-figure 8) shows presence of cells throughout the sample, not just in the regions near the flow channel edge. Since the calcified environment along the formed along the channel serves absorbs the Fluo4 dye, preventing its diffusion in zone 2, we only focused on zone 1 within this experiment. Our results show a significant reduction of the single peak cells (figure 7(e)) with yet only modest changes to the slow, plateau and inactive populations in zone 1 when co-cultured with mineralizing osteoblasts. It is also worth noting that, as shown in our experiments presented as figure 4, that greatest changes observed in response to fluid shear stimuli under the matrix confinement conditions occurred in Zone 2 (figure 4). Unfortunately, in the co-culture experiment, our ability to detect Ca^{2+} in zone 2 was confounded by the absorption of the Fluo4 stain by the calcified matrix in zone 1, precluding its diffusion to zone 2. Based on the confocal imaging data, we assume that there are relatively few heterotypic (osteocyte:osteoblast) junctions in our experiment as the majority of the osteoblastic cells were suspended in the GelMA layer above the osteocyte monolayer. Possibly, with longer culture times, osteoblasts (SaoS-2) could migrate and form several osteoblast-osteocyte contacts, but this was not investigated in this work. Confounding effect of Fluo4 dye retention in the calcified environment as a

technical barrier to observing Ca^{2+} dynamics in zone 2 of this model system.

4. Materials and methods

4.1. Cell culture and procedure for flow stimulation

Murine osteocyte-like cell line MLO-Y4 (Kerafast, Inc. Boston, MA) were cultured according to the suppliers recommended protocol [76]. The cell culture flasks were coated with $4 \mu\text{g cm}^{-2}$ rat tail type I collagen (Sigma-Aldrich, Inc. St. Louis, MO) for 30 min at 37°C before cell seeding. Alpha-Minimum Essential Media (Thermo-Fisher Scientific, Grand Island, NY) supplemented with 2.5% fetal bovine serum (FBS, R&D Systems, Minneapolis, MN), 2.5% calf serum (Cytiva Life Sciences, Marlborough, MA) and 1% penicillin/streptomycin (Thermo-Fisher Scientific) were used as cell culture media. The cells were seeded on collagen coated glass slides (Fisherbrand, Thermo-Fisher Scientific) at a density of $10\,000 \text{ cells cm}^{-2}$ and cultured for a period of 1–3 days. Human osteoblast like Saos2 osteosarcoma cells (ATCC, Manassas, VA) were cultured with Dulbecco's modification of eagle's media (DMEM, Thermo-Fisher Scientific supplemented with 10% FBS (R&D Systems)), 1% penicillin/streptomycin (Thermo-Fisher Scientific) and 1% Glutamax (Thermo-Fisher Scientific) using standard cell culture protocol.

4.2. Flow stimulation

Clear polycarbonate was used to create a flow chamber that accommodates standard glass microscope slide. The chamber consists of a top plate ($90 \times 40 \times 6.35 \text{ mm}$). Threaded barbed fittings were attached to the top plate to allow for silicone tubing to be attached. A computer numerical control (CNC) was used to mill openings on the bottom plate to facilitate high-resolution imaging. A pocket was machined with the exact dimensions of the glass slide to allow for a tight fit and to ensure the top surface of the slide aligns with the top surface of the bottom plate (SI, figure 1(A)). A commercially available laser cutter was used to cut a high-purity high-temperature silicone rubber gasket (thickness = $254 \mu\text{m}$, 0.010 inch). The height of the flow chamber ($254 \mu\text{m}$) was generated by inserting the gasket between top and bottom plates. These flow chambers were used without modification to establish the 'nonconfined' condition.

To generate 'confined' condition, GelMA hydrogel was spatially photo-crosslinked on top of osteocyte monolayers, seeded on glass slides at a density of 10^5 cm^{-2} one day for 24 h before flow stimulation was applied. Briefly, cells were first loaded with calcium indicator, then assembled into the chamber and confined with GelMA.

GelMA prepolymer was synthesized according to our previous work [77]. Briefly, 10% (w/v)

GelMA prepolymer solution with 0.5% (v/v) - Lithium phenyl-2,4,6-trimethylbenzoylphosphinate (LAP) was perfused in the flow chamber within the assembled flow chamber. Prior to UV crosslinking, the chamber was placed in a 3D printed, acrylonitrile butadiene (ABS) plastic frame with a 7 mm wide mask, ensuring selective crosslinking of GelMA walls on either side of a central 7 mm wide flow channel (SI, figure 1(B)). GelMA was crosslinked at 395 nm 40 mW cm^{-2} for 15 s. After crosslinking, the chamber inlet was connected to a syringe pump and culture media was perfused into the chamber to remove non-crosslinked GelMA, leaving central channel flanked by crosslinked GelMA on either side. Then, the channel was perfused with 0.05% trypsin solution, incubated for 5 min at static to dislodge the cells, and media was perfused to remove them from the flow channel. Since 10% GelMA maintains its structural stability for several weeks after UV crosslinking, this formulation was chosen for this study [78].

Prior to flow-stimulation, the cells were loaded with Fluo-4 Ca^{2+} imaging dye (Thermo-Fisher Scientific) for 20 min at 37°C , followed by 20 min at room temperature before starting the fluid flow stimulation. The experiments were conducted at room temperature. Fluorescence data recorded at 120 fpm for 30 s under static flow conditions was used as a baseline control (no flow stimulation). The media perfusion was started from 30 s to 200 s at a flow rate of 700 ml h^{-1} for cells under nonconfined conditions and 250 ml h^{-1} for cells for cells under confined conditions; the flow rates were varied based on the cross-section of the channel to ensure identical shear stress under both conditions. The shear stress was calculated to be $\sim 0.85 \text{ Pa}$ using the following equation: $= \frac{6\mu Q}{wh^2}$, where μ is the viscosity of fluid, Q is the flow rate, w is the width of channel and h is the height of the channel. This was further confirmed by computational modeling (SI figure 7). For both confined and unconfined conditions, the flow was applied from 30 to 200 s, while Ca^{2+} response was recorded for either 200 or 600 s. Two rounds of flow stimulation were performed on the same sample with a rest duration of 10 min between rounds.

To establish more physio-mimetic conditions of confinement within a bone-like mineralized matrix, for some experiments, Saos2 ($4 \times 10^6 \text{ ml}^{-1}$) were encapsulated in the GelMA on top of osteocyte monolayer and this setup was cultured for seven days to provide a mineralized bone-like confining matrix. Prior to flow experiments, the Saos2 cells were induced to mineralization by perfusing the flow chamber with DMEM supplemented with $100 \mu\text{M}$ L-ascorbic acid-2-phosphate (Sigma-Aldrich) and 5 mM β -glycerophosphate (Sigma-Aldrich) at 0.4 ml h^{-1} for seven days. Prior to imaging these experiments, the chamber was than loaded with Fluo-4 Ca^{2+} solution for 3 h before imaging. After

imaging, the chamber was rinsed with phosphate buffer saline (PBS) and filled with 4% paraformaldehyde (Sigma) at 4°C overnight for fixation, before perfusing with Alizarin red staining solution (Sigma) for 5 min and rinsing with PBS three times to verify Ca^{2+} mineral deposition by the suspended Saos2 cells. The MLO-Y4 cells were stained with DiI C_{12} (3) (Thermo-Fisher Scientific) and the Saos2 cells were stained with DiOC $_{18}$ (3) (Thermo-Fisher Scientific) before being seeded and encapsulated. The flow chamber was perfused for three days with osteogenic media. The chamber was then imaged using Zeiss LSM780 confocal microscope.

For Ca^{2+} free experiment, minimal essential medium (MEM) (Thermo-Fisher Scientific) without Ca^{2+} was used for flow stimulation. For gap junction inhibitor experiments, 18-GA ($80 \mu\text{M}$, Sigma) was added to the Fluo-4 loading solution. Time-lapse images were taken every 500 ms with Nikon Eclipse Ti microscope, S Plan Fluor ELWD $20\times$ Ph1 ADM, FilterChanger GFPHQ with a Zyla 4.2 Plus sCMOS camera (Nikon, Melville, NY).

4.3. Image processing and statistical analysis

Ca^{2+} signal intensity was quantified with ImageJ. Each cell was selected as a region of interest for intensity measurement. The intensity of first 30 s were averaged to generate a baseline F_0 . Then intensity of each frame was divided by baseline to get normalized value F/F_0 . The maximum peak intensity, half peak, FWHM, time to peak, peak interval and final intensity were defined (SI figure 2). For cellular response under fluid flow stimulation, (a) signals with FWHM less than 120 s were defined as 'single peak', (b) signals with two or more peaks with FWHM less than 120 s were defined as 'multi-peak', (c) signals with FWHM greater than 120 s were defined as 'slow recovery', (d) signals that exhibit linear increase in fluorescent intensity during the 200 s slow stimulus and flatlines until 600 s were defined as 'plateau', and (e) signals with F/F_0 less than 1.05 were defined as 'inactive'. To estimate influence of proximity of osteocytes to fluid stimuli, a zonal analysis was also performed where zone 1 and 2 were defined as regions that are $0\text{--}200 \mu\text{m}$ and $200\text{--}400 \mu\text{m}$ from the edge of perfusion channel. Experiments were repeated three times for each condition. All the cells in time-lapse images were quantified for fluorescence intensity. Only cells with flat baseline in the first 30 s were selected for further analysis. Descriptive statistics were calculated in Microsoft Excel and two-tailed Student's t-test was performed to determine significant difference in Prism, where $p < 0.05$ was accepted as significant.

4.4. Immunofluorescence staining

The cells within the flow chambers were fixed with 4% paraformaldehyde (Sigma) for 20 min, permeabilized with 0.1% Triton X-100 (Sigma) for 20 min

and blocked with 1% bovine serum albumin (Sigma) for 1 h. Then, cells were labeled with a rabbit-anti Connexin 43 polyclonal antibody ($2 \mu\text{g ml}^{-1}$, Invitrogen 71-0700) overnight at 4°C , followed by Alexa Fluor 647 goat-anti rabbit secondary antibody (Invitrogen) and Alexa Fluor 568 phalloidin (Invitrogen) at 1:100 for 1 h at room temperature. Cells were incubated in $0.5 \mu\text{g ml}^{-1}$ 4',6-diamidino-2-phenylindole (DAPI) solution (Invitrogen) for 5 min for nuclei staining. Images were taken with either Nikon Eclipse Ti microscope or Zeiss LSM780 confocal microscope. To quantify the cellular connection in the network, two cell dendrites contacting with a Cx43+ channel was defined as one connection. Connections formed by each cell were counted to generate a histogram connection distribution.

4.5. Simulation of shear stress

A two-dimensional (2D) finite element model to simulate the stress distribution in the gel strip subjected to shear traction loading at the interface between the solid and fluid was applied. As shown in SI-figure 7, the modeled hydrogel strip has a length of 69 mm and thickness of 6 mm. The left, top, and bottom surfaces are perfectly bonded to the walls. The right surface is adjacent to the fluid flow stimuli. Based on the flow channel dimension and flow rate, we estimate the shear stress at the gel surface is 0.85 Pa, which was prescribed as a shear traction boundary condition in the simulations. The deformation of the hydrogel strip was assumed to be under plane-strain condition. The elastic properties and energy dissipation of the hydrogel were modeled as the fully incompressible neo-Hookean material with Young's modulus as 15 kPa (modulus of 7% GelMA). All the numerical simulations were carried out with ABAQUS/Implicit. The hydrogel was modeled with CPE4R element. We adopted a fine mesh size (0.2 mm) to capture the spatial distribution of the stress inside the gel.

Data availability statement

All data that support the findings of this study are included within the article (and any supplementary files).

Acknowledgments

We gratefully acknowledge funding from NIH R21AR076642.

ORCID iDs

Jason A Horton  <https://orcid.org/0000-0003-3396-5063>

Pranav Soman  <https://orcid.org/0000-0001-9456-0030>

References

- [1] Schaffler M B, Cheung W-Y, Majeska R and Kennedy O 2014 Osteocytes: master orchestrators of bone *Calcif. Tissue Int.* **94** 5–24
- [2] Gasser J A and Kneissel M 2017 *Bone Physiology and Biology, Bone Toxicology* (Berlin: Springer) pp 27–94
- [3] Kerschnitzki M, Kollmannsberger P, Burghammer M, Duda G N, Weinkamer R, Wagermaier W and Fratzl P 2013 Architecture of the osteocyte network correlates with bone material quality *J. Bone Miner. Res.* **28** 1837–45
- [4] York S, Sethu P and Saunders M 2016 Impact of gap junctional intercellular communication on MLO-Y4 sclerostin and soluble factor expression *Ann. Biomed. Eng.* **44** 1170–80
- [5] Fritton S P and Weinbaum S 2009 Fluid and solute transport in bone: flow-induced mechanotransduction *Annu. Rev. Fluid Mech.* **41** 347–74
- [6] Wang B, Sun X, Akkus O and Wang L 2018 Elevated solute transport at sites of diffuse matrix damage in cortical bone: implications on bone repair *J. Orthop. Res.* **36** 692–8
- [7] Cheng B, Zhao S, Luo J, Sprague E, Bonewald L F and Jiang J X 2001 Expression of functional gap junctions and regulation by fluid flow in osteocyte-like MLO-Y4 cells *J. Bone Miner. Res.* **16** 249–59
- [8] Cowin S C and Cardoso L 2015 Blood and interstitial flow in the hierarchical pore space architecture of bone tissue *J. Biomech.* **48** 842–54
- [9] Burger E and Klein-Nulend J 1999 Responses of bone cells to biomechanical forces *in vitro Adv. Dent. Res.* **13** 93–98
- [10] Gkotsamanidou M, Dimopoulos M A, Kastiris E, Christoulas D, Mouloupoulos L A and Terpos E 2012 Sclerostin: a possible target for the management of cancer-induced bone disease *Expert Opin. Ther. Targets* **16** 761–9
- [11] Sezer O, Heider U, Zavrski I, Kühne C A and Hofbauer L C 2003 RANK ligand and osteoprotegerin in myeloma bone disease *Blood* **101** 2094–8
- [12] Wijenayaka A R, Kogawa M, Lim H P, Bonewald L F, Findlay D M and Atkins G J 2011 Sclerostin stimulates osteocyte support of osteoclast activity by a RANKL-dependent pathway *PLoS One* **6** e25900
- [13] Balemans W, Ebeling M, Patel N, Van Hul E, Olson P, Dioszegi M, Lacza C, Wuyts W, Van Den Ende J and Willems P 2001 Increased bone density in sclerosteosis is due to the deficiency of a novel secreted protein (SOST) *Hum. Mol. Genet.* **10** 537–44
- [14] Schindeler A, McDonald M M, Bokko P and Little D G 2008 *Bone Remodeling during Fracture Repair: The Cellular Picture* (Amsterdam: Elsevier) pp 459–66
- [15] Zhang Y, Yan M, Yu A, Mao H and Zhang J 2012 Inhibitory effects of beta-tricalciumphosphate wear particles on osteocytes via apoptotic response and Akt inactivation *Toxicology* **297** 57–67
- [16] Li X, Warmington K S, Niu Q T, Asuncion F J, Barrero M, Grisanti M, Dwyer D, Stouch B, Thway T M and Stolima M 2010 Inhibition of sclerostin by monoclonal antibody increases bone formation bone mass, and bone strength in aged male rats *J. Bone Miner. Res.* **25** 2647–56
- [17] Aono Y, Yamazaki Y, Yasutake J, Kawata T, Hasegawa H, Urakawa I, Fujita T, Wada M, Yamashita T and Fukumoto S 2009 Therapeutic effects of anti-FGF23 antibodies in hypophosphatemic rickets/osteomalacia *J. Bone Miner. Res.* **24** 1879–88
- [18] Weinstein R S, Jilka R L, Almeida M, Roberson P K and Manolagas S C 2010 Intermittent parathyroid hormone administration counteracts the adverse effects of glucocorticoids on osteoblast and osteocyte viability, bone formation, and strength in mice *Endocrinology* **151** 2641–9
- [19] Compton J T and Lee F Y 2014 A review of osteocyte function and the emerging importance of sclerostin *J. Bone Joint Surg. Am.* **96** 1659–68

- [20] Bonewald L F 2011 The amazing osteocyte *J. Bone Miner. Res.* **26** 229–38
- [21] Knothe T M L, Niederer P and Knothe U 1998 *In vivo* tracer transport through the lacunocanalicular system of rat bone in an environment devoid of mechanical loading *Bone* **22** 107–17
- [22] Köhler A, Schmithorst V, Filippi M-D, Ryan M A, Daria D, Gunzer M and Geiger H 2009 Altered cellular dynamics and endosteal location of aged early hematopoietic progenitor cells revealed by time-lapse intravital imaging in long bones *Blood* **114** 290–8
- [23] Hinton P V, Rackard S M and Kennedy O D 2018 *In vivo* osteocyte mechanotransduction: recent developments and future directions *Curr. Osteoporos. Rep.* **16** 746–53
- [24] Buenzli P R and Sims N A 2015 Quantifying the osteocyte network in the human skeleton *Bone* **75** 144–50
- [25] Tanaka T, Hoshijima M, Sunaga J, Nishida T, Hashimoto M, Odagaki N, Osumi R, Aadachi T and Kamioka H 2018 Analysis of Ca^{2+} response of osteocyte network by three-dimensional time-lapse imaging in living bone *J. Bone Miner. Metab.* **36** 519–28
- [26] Morrell A E, Brown G N, Robinson S T, Sattler R L, Baik A D, Zhen G, Cao X, Bonewald L F, Jin W and Kam L C 2018 Mechanically induced Ca^{2+} oscillations in osteocytes release extracellular vesicles and enhance bone formation *Bone Res.* **6** 6
- [27] Lewis K J, Frikha-Benayed D, Louie J, Stephen S, Spray D C, Thi M M, Seref-Ferlengez Z, Majeska R J, Weinbaum S and Schaffler M B 2017 Osteocyte calcium signals encode strain magnitude and loading frequency *in vivo Proc. Natl Acad. Sci.* **114** 11775–80
- [28] You L, Temiyasathit S, Tao E, Prinz F and Jacobs C R 2008 3D microfluidic approach to mechanical stimulation of osteocyte processes *Cell Mol. Bioeng.* **1** 103–7
- [29] Mei X, Middleton K, Shim D, Wan Q, Xu L, Ma Y-H V, Devadas D, Walji N, Wang L and Young E W 2019 Microfluidic platform for studying osteocyte mechanoregulation of breast cancer bone metastasis *Integr. Biol.* **11** 119–29
- [30] Yvanoff C and Willaert R G 2022 Development of bone cell microarrays in microfluidic chips for studying osteocyte–osteoblast communication under fluid flow mechanical loading *Biofabrication* **14** 025014
- [31] Xu L H 2021 *Novel in Vitro Microfluidic Platform for Studying Osteocyte Mechanobiology* (Toronto: University of Toronto)
- [32] George E L, Truesdell S L, York S L and Saunders M M 2018 Lab-on-a-chip platforms for quantification of multicellular interactions in bone remodeling *Exp. Cell Res.* **365** 106–18
- [33] York S L, Arida A R, Shah K S, Sethu P and Saunders M M 2012 Osteocyte characterization on polydimethylsiloxane substrates for microsystems applications *J. Biomim. Biomater. Tissue Eng.* **16** 27–42
- [34] Zhang W, Gu Y, Hao Y, Sun Q, Konior K, Wang H, Zilberberg J and Lee W 2015 Well plate-based perfusion culture device for tissue and tumor microenvironment replication *Lab Chip* **15** 2854–63
- [35] Iordachescu A, Amin H D, Rankin S M, Williams R L, Yapp C, Bannerman A, Pacureanu A, Addison O, Hulley P A and Grover L M 2018 An *in vitro* model for the development of mature bone containing an osteocyte network *Adv. Biosyst.* **2** 1700156
- [36] Kurata K, Heino T J, Higaki H and Väänänen H K 2006 Bone marrow cell differentiation induced by mechanically damaged osteocytes in 3D gel-embedded culture *J. Bone Miner. Res.* **21** 616–25
- [37] Honma M, Ikebuchi Y, Kariya Y and Suzuki H 2015 Establishment of optimized *in vitro* assay methods for evaluating osteocyte functions *J. Bone Miner. Metab.* **33** 73–84
- [38] Sun Q, Choudhary S, Mannion C, Kissin Y, Zilberberg J and Lee W Y 2017 Ex vivo construction of human primary 3D-networked osteocytes *Bone* **105** 245–52
- [39] Gu Y, Zhang W, Sun Q, Hao Y, Zilberberg J and Lee W Y 2015 Microbead-guided reconstruction of the 3D osteocyte network during microfluidic perfusion culture *J. Mater. Chem. B* **3** 3625–33
- [40] Boukhechba F, Balaguer T, Michiels J F, Ackermann K, Quincey D, Boulter J M, Pyerin W, Carle G F and Rochet N 2009 Human primary osteocyte differentiation in a 3D culture system *J. Bone Miner. Res.* **24** 1927–35
- [41] Sun Q, Choudhary S, Mannion C, Kissin Y, Zilberberg J and Lee W Y 2018 Ex vivo replication of phenotypic functions of osteocytes through biomimetic 3D bone tissue construction *Bone* **106** 148–55
- [42] Choudhary S, Sun Q, Mannion C, Kissin Y, Zilberberg J and Lee W Y 2018 Hypoxic three-dimensional cellular network construction replicates ex vivo the phenotype of primary human osteocytes *Tissue Eng. A* **24** 458–68
- [43] Dallas S L and Moore D S 2020 Using confocal imaging approaches to understand the structure and function of osteocytes and the lacunocanalicular network *Bone* **138** 115463
- [44] Bonewald L F 1999 Establishment and characterization of an osteocyte-like cell line, MLO-Y4 *J. Bone Miner. Metab.* **17** 61–65
- [45] Purvis J E and Lahav G 2013 Encoding and decoding cellular information through signaling dynamics *Cell* **152** 945–56
- [46] Berridge M J, Bootman M D and Roderick H L 2003 Calcium signalling: dynamics, homeostasis and remodelling *Nat. Rev. Mol. Cell Biol.* **4** 517–29
- [47] Weinbaum S, Cowin S C and Zeng Y 1994 A model for the excitation of osteocytes by mechanical loading-induced bone fluid shear stresses *J. Biomech.* **27** 339–60
- [48] Qin L, Liu W, Cao H and Xiao G 2020 Molecular mechanosensors in osteocytes *Bone Res.* **8** 1–24
- [49] Temiyasathit S and Jacobs C R 2010 Osteocyte primary cilium and its role in bone mechanotransduction *Ann. New York Acad. Sci.* **1192** 422–8
- [50] Leybaert L and Sanderson M J 2012 Intercellular Ca^{2+} waves: mechanisms and function *Physiol. Rev.* **92** 1359–92
- [51] Clapham D E 2007 Calcium signaling *Cell* **131** 1047–58
- [52] Kwon R Y and Jacobs C R 2007 Time-dependent deformations in bone cells exposed to fluid flow *in vitro*: investigating the role of cellular deformation in fluid flow-induced signaling *J. Biomech.* **40** 3162–8
- [53] Ponik S M, Triplett J W and Pavalko F M 2007 Osteoblasts and osteocytes respond differently to oscillatory and unidirectional fluid flow profiles *J. Cell. Biochem.* **100** 794–807
- [54] Lu X L, Huo B, Park M and Guo X E 2012 Calcium response in osteocytic networks under steady and oscillatory fluid flow *Bone* **51** 466–73
- [55] Jing D, Lu X L, Luo E, Sajda P, Leong P L and Guo X E 2013 Spatiotemporal properties of intracellular calcium signaling in osteocytic and osteoblastic cell networks under fluid flow *Bone* **53** 531–40
- [56] Donahue S W, Jacobs C R and Donahue H J 2001 Flow-induced calcium oscillations in rat osteoblasts are age, loading frequency, and shear stress dependent *Am. J. Physiol. Cell Physiol.* **281** C1635–41
- [57] Sawyer S W, Zhang K, Horton J A and Soman P 2020 Perfusion-based co-culture model system for bone tissue engineering *AIMS Bioeng.* **7** 91–105
- [58] Sawyer S W, Shridhar S V, Zhang K, Albrecht L D, Filip A B, Horton J A and Soman P 2018 Perfusion directed 3D mineral formation within cell-laden hydrogels *Biofabrication* **10** 035013
- [59] Ramos R, Zhang K, Quinn D, Sawyer S W, McLoughlin S and Soman P 2019 Measuring changes in electrical impedance during cell-mediated mineralization *Bioelectricity* **1** 73–84
- [60] Jing D, Baik A D, Lu X L, Zhou B, Lai X, Wang L, Luo E and Guo X E 2014 *In situ* intracellular calcium oscillations in osteocytes in intact mouse long bones under dynamic mechanical loading *FASEB J.* **28** 1582–92

- [61] Adachi T, Aonuma Y, Ito S I, Tanaka M, Hojo M, Takano-Yamamoto T and Kamioka H 2009 Osteocyte calcium signaling response to bone matrix deformation *J. Biomech.* **42** 2507–12
- [62] Molineux M L, McRory J E, McKay B E, Hamid J, Mehaffey W H, Rehak R, Snutch T P, Zamponi G W and Turner R W 2006 Specific T-type calcium channel isoforms are associated with distinct burst phenotypes in deep cerebellar nuclear neurons *Proc. Natl Acad. Sci.* **103** 5555–60
- [63] Dockrell M E, Noor M I, James A F and Hendry B M 2001 Heterogeneous calcium responses to extracellular ATP in cultured rat renal tubule cells *Clin. Chim. Acta* **303** 133–8
- [64] Hong D, Barbee K, Buerk D and Jaron D Heterogeneous cytoplasmic calcium response in microvascular endothelial cells 2005 *IEEE Engineering in Medicine and Biology 27th Annual Conf.* (IEEE) pp 7493–6
- [65] Wiltink A, van den Brink A M, Herrmann-Erlee M, Van der Meer J, Van der Plas A, Willems P, Van Duijn B, Nijweide P and Ypey D 1993 Heterogeneity of intracellular calcium responses to parathyroid hormone and thrombin in primary osteoblast-like cells and UMR106-01 cells: correlations with culture conditions, intracellular calcium concentration and differentiation state *Cell Calcium* **14** 591–600
- [66] Duncan R L and Turner C H 1995 Mechanotransduction and the functional response of bone to mechanical strain *Calcif. Tissue Int.* **57** 344–58
- [67] Wittkowske C, Reilly G C, Lacroix D and Perrault C M 2016 *In vitro* bone cell models: impact of fluid shear stress on bone formation *Front. Bioeng. Biotechnol.* **4** 87
- [68] Rawlinson S, Pitsillides A and Lanyon L 1996 Involvement of different ion channels in osteoblasts' and osteocytes' early responses to mechanical strain *Bone* **19** 609–14
- [69] Mikuni-Takagaki Y 1999 Mechanical responses and signal transduction pathways in stretched osteocytes *J. Bone Miner. Metab.* **17** 57–60
- [70] Loisel A E, Jiang J X and Donahue H J 2013 Gap junction and hemichannel functions in osteocytes *Bone* **54** 205–12
- [71] Genetos D C, Kephart C J, Zhang Y, Yellowley C E and Donahue H J 2007 Oscillating fluid flow activation of gap junction hemichannels induces ATP release from MLO-Y4 osteocytes *J. Cell. Physiol.* **212** 207–14
- [72] Deepak V, Kayastha P and McNamara L M 2017 Estrogen deficiency attenuates fluid flow-induced $[Ca^{2+}]_i$ oscillations and mechanoresponsiveness of MLO-Y4 osteocytes *FASEB J.* **31** 3027–39
- [73] Brown G N, Sattler R L and Guo X E 2016 Experimental studies of bone mechanoadaptation: bridging *in vitro* and *in vivo* studies with multiscale systems *Interface Focus* **6** 20150071
- [74] Williams K M, Leser J M, Gould N R, Joca H C, Lyons J S, Khairallah R J, Ward C W and Stains J P 2020 TRPV4 calcium influx controls sclerostin protein loss independent of purinergic calcium oscillations *Bone* **136** 115356
- [75] Li X, Han L, Nookaew I, Mannen E, Silva M J, Almeida M and Xiong J 2019 Stimulation of Piezo1 by mechanical signals promotes bone anabolism *Elife* **8** e49631
- [76] Kato Y, Windle J J, Koop B A, Mundy G R and Bonewald L F 1997 Establishment of an osteocyte-like cell line, MLO-Y4 *J. Bone Miner. Res.* **12** 2014–23
- [77] Albrecht L D, Sawyer S W and Soman P 2016 Developing 3D scaffolds in the field of tissue engineering to treat complex bone defects *3D Print. Addit. Manuf.* **3** 106–12
- [78] Sawyer S, Oest M, Margulies B and Soman P 2016 Behavior of encapsulated Saos-2 cells within gelatin methacrylate hydrogels *J. Tissue Sci. Eng.* **7** 2